MISSOURI S&T

Missouri University of Science and Technology

Scholars' Mine

International Specialty Conference on Cold-Formed Steel Structures

(2002) - 16th International Specialty Conference on Cold-Formed Steel Structures

Oct 17th, 12:00 AM

Design of Industrial Storage Racks

Andrew T. Sarawit

Teoman Pekoz

Follow this and additional works at: https://scholarsmine.mst.edu/isccss

⚙ Part of the Structural Engineering Commons

Recommended Citation

DESIGN OF INDUSTRIAL STORAGE RACKS

A. T. Sarawit[1], T. Peköz[2]

ABSTRACT

Design of industrial steel storage racks is complex due to the presence of significant perforations in the columns and the semi-rigid nature of column bases and beam to column connections. Many assumptions are made in the current design provisions to simplify the design but as a result the design becomes rather conservative. Studies were conducted at both the component and global scale to address some of these assumptions. At the component level, the topics focused upon are the column bases, beam to column connections, and members. Results indicate that improvements in the current design procedures are possible and recommendations for improvement are made.

1   INTRODUCTION

The behavior of the components: column bases, beam to column connections, and members have a significant effect on the performance of the industrial storage racks. The current design provisions in the RMI (1997) specifications for industrial steel storage racks, recommend the use of a base fixity equation and beam to column connection tests to account for the semi-rigid nature of the column bases and beam to column connection. Also stub column tests are required to account for the local behavior of the members because no satisfactory theoretical treatment has yet been developed to deal with the presence of perforations in the column section. Studies were first carried out for each of these components then followed by a study on cold-formed steel frames. A critical review of the current design provisions was carried out in these studies to verify or modify the design approach.

2   COLUMN BASES

The RMI specification uses the following base fixity expression for the ratio of the moment with respect to the corresponding rotation of the base as

$$\frac{M}{\theta} = \frac{bd^2 E_c}{12} \qquad (2.1)$$

where b is the width of the column parallel to the flexural axis, d is the depth of the column perpendicular to the flexural axis, and E_c is the modulus of elasticity of the floor assumed to be concrete. The expression above is based on an analytical approximation developed by Salmon, Schenker and Johnston (1955). The base fixity obtained from this expression is equivalent to

---

[1] Graduate Research Assistant, School of Civil and Environmental Engineering, Cornell University, Ithaca, NY 14853, U.S.A.
[2] Professor, School of Civil and Environmental Engineering, Cornell University, Ithaca, NY 14853, U.S.A.

assuming that the concrete block under the base plate is subject to a bending load distribution as shown in Fig. 2.1. Forces in the column, which transfer through the base plate and then onto the concrete surface, can be considered as a combination of an axial and bending force. However, only the bending force contributes to the rotation of the base. Considering only the concrete block under the base plate, however, results in a lower stiffness than what the actual floor could develop. This is because the model neglects the confinement from the surrounding material. The concrete floor should instead be represented by a half-space material. Based on this idea studies were carried out to develop a new base fixity equation.

2.1   Development of a Base Fixity Equation

Finite element studies of the base fixity problem have shown that contact pressures between the base plate and concrete surface are concentrated around the column wall section rather than having a linear bending load distribution as assumed in Eq. (2.1). This is because the column wall thickness t_w and base plate thickness t_p in study are relatively thin compared to the width or depth of the column. The distribution of the normal loads on the concrete surface depends on these thicknesses and the location of the column wall section on the base plate. An example of approximate load distributions for a C-section with different types of base plate configurations is shown in Fig. 2.2. As expected the load is distributed wider when the column wall section is located at the center of the base plate rather than when it is located at the edges.

   Once the normal load distribution on the concrete surface for a certain amount of bending moment is known, deformation of the concrete can be obtained by solving the problem of normal loads on the boundary of the half-space using solid mechanic approaches as suggested in Sokolnikoff (1983). The rotation is found from the surface deformation, and then the base fixity is computed. A parametric study is carried out for a wide range of parameters as summarized in Table 2.1. Combinations of these parameters yield a total of 900 models for each base plate type. Results are shown in Figs. 2.3a and 2.3b. It is found that the results of base plate type A are similar to type B while the results of base plate type C are similar to type D. This is mainly because the load at the stiffener and web is rather low. Most of the rotation takes place due to the loads from flanges. New base fixity equations can now be obtained by fitting a regression line through the resulting data. For use with base plate type A or B, the proposed equation is

$$\frac{M}{\theta} = \frac{7}{25} bd^2 E_c \tag{2.2}$$

For use with base plate type C or D, the proposed equation is

$$\frac{M}{\theta} = \frac{7}{20} bd^2 E_c \tag{2.3}$$

The base fixity equations presented here are suggested only for the initial stiffness, namely, only when the base plate is still in full contact with the concrete surface, having compression stress distribution. By considering the axial force, P and bending moment M at the column base, to prevent tension stresses from occurring, an upper bound limit of the equations can be found as

$$\frac{M}{P} \leq \frac{S}{A} \tag{2.4}$$

where A is the cross sectional area of the column and S is the elastic section modulus of the column section for the extreme tension fiber about the axis of bending. Once the upper bound limitation has been reached, the stiffness of the connection is expected to decrease.

2.2   Finite Element Analysis Verification

Non-linear finite element analyses of the column to floor connection are performed using ABAQUS in order to verify the proposed base fixity equation. The finite element model is shown in Fig. 2.4 and assumptions are as follows. The vertical and lateral loads transferred from the frame to the isolated column are modeled by nodal forces applied at the centroid of the column on the top plate. The ratio of the lateral load with respect to the vertical load is maintained through the analysis. Lateral bracing is provided at the top plate to prevent the column from twisting. In addition, because only one anchorage bolt is chosen for this model, it is expected that the placement of the bolts will affect the behavior of the column. Therefore, both directions of the lateral load must be considered. Positive and negative signs of the direction are given in Fig. 2.4. An idealization of the boundary conditions of the anchorage bolts connection is made by the matching displacements of the base plate nodes and the concrete surface nodes.

The four node general purpose shell element is used to model the column and base plate while an eight node brick element is used to model the concrete floor. Contact surfaces are defined between the base plate and the concrete to simulate their interaction. However, in this study no friction is considered between the two surfaces. In addition, since the floor is assumed to be a half-space, eight node infinite elements are needed to model the far-field region. The material model used for the column and base plate is elastic-plastic with strain hardening $F_y = 45$ ksi, $F_u = 59$ ksi, $E = 29500$ ksi, and $v = 0.3$ while the concrete is assumed elastic with $E_c = 2950$ ksi and $v = 0.2$. The rotation of the base plate is obtained and plotted against the applied moment to compare with the proposed equation as shown in Fig. 2.5. It can be seen that the proposed equation for base plate type A and B agrees well with the finite element solution.

3   BEAM TO COLUMN CONNECTIONS

In storage racks, beam end connectors are used to make beam to column connections. The semi-rigid nature of this connection is due to the distortion of the column walls, tearing of the column perforation and distortion of the beam end connector. Storage rack stability depends significantly on the behavior of the beam to column connection, thus it is important to have the means for predicting it. Designs of these connections vary widely; therefore, it is impossible to develop a general analytic model. Instead, beam to column connection tests are usually done to determine the relationship of the moment at the joint M and the change in angle between the column and the connecting beam θ. The RMI specification recommends the use of a cantilever test or a portal test. Schematics of these test setups are shown in Fig 3.1 and 3.2. In the cantilever test the constant connection stiffness F relating the moment to the rotation as

$$F = \frac{M}{\theta} \tag{3.1}$$

is determined by using the known applied vertical load and deflection of the free end of the cantilever. While in the portal test, a certain amount of vertical load is first applied. Then by applying an additional horizontal load and measuring the corresponding lateral deflection the constant connection stiffness can be determined. The moment and rotation relationship determined from the cantilever test is normally used for the design of beams and connections while the result from the portal test it is used as connection stiffness in sidesway analyses.

An alternative beam to column connection test is presented here to be used instead of the cantilever test. In the cantilever test the shear to moment ratio of the actual frames may not be well represented. Namely, if the cantilever test is conducted for different lengths of the cantilever beam, the moment and rotation relationships obtained from each of these tests might be different. To solve this problem a proposed connection test where the entire bay is assembled the same as in the portal test is to be used. This test is similar to the portal test but instead of applying the horizontal loads, vertical loads are applied incrementally and the corresponding mid span beam deflection δ is measured. The vertical load applied must be equally distributed over the entire bay so that the force on each shelf beam can be assumed to be a uniformly distributed vertical load w. The developing moment in each joint will be the same in this test and the expression for F can be found as follows:

$$F = \cfrac{1}{\cfrac{L}{2EI_b}\left(\cfrac{4wL^4}{5wL^4 - 384EI_b\delta} - 1\right) - \cfrac{h}{3EI_c}}$$
(3.2)

where I_b and I_c are the moments of inertia of the beam and column segment. The corresponding moments developed in the joints can be found as follows:

$$M = \cfrac{wL^3}{24EI_b\left(\cfrac{h}{3EI_c} + \cfrac{L}{2EI_b} + \cfrac{1}{F}\right)}$$
(3.3)

To obtain the moment and rotation relationships, θ can be determined for each load step using Eq. (3.1). The load carrying capacity of the entire bay may also be determined from this test whether failure is due to the connection or the shelf beam. However, if the load carrying capacity is not of interest, the proposed test could be conducted prior to the portal test.

4   MEMBERS

4.1   Elastic Buckling Strength

The column sections in storage racks are perforated for the purpose of easy assembly of the beam end connector. It is well known that the presence of such perforation reduces the buckling strength of the section. The significance of this reduction will however depend on the geometry and material properties of the member and the boundary conditions. The RMI specification allows the use of the full cross section properties to predict the overall buckling strength, thus assuming that the presence of such perforation does not have significant influence on the overall buckling strength. The objective of this study is to validate this assumption.

A study is carried out to compare the buckling strengths of perforated and unperforated A-LDR type columns. The cross sectional geometry is shown in Fig 4.1. Two section thicknesses are investigated, one where the section is locally stable, which in this study will be referred to as the thick-walled section and the other where the section is locally unstable under yield stress, which will be referred to as the thin-walled section. These sections are studied as both a concentrically loaded compression member and a flexural member subject to bending about the strong axis. Boundary conditions at the ends of the member for both cases are pined condition such that the effective lengths for bending about of both the strong and weak axes and torsion are equal to the length of the member. The critical buckling load is found for the different length

members. Two approaches are used and then compared: finite element method using the ABAQUS computer program and the theoretical overall buckling equations as given in the AISI (1996) specification. The finite element method is considered to give more accurate results.

Finite element models range from a member length of 12 to 120 in. with a 6 in. increment between models. The theoretical values are obtained for the full section, weighted section, and in addition the net section moment of inertia for the flexural buckling mode. A weighted section as shown in Fig. 4.1 refers to a section that uses an average thickness in the perforated segment of the section to account for the absence of the material from the holes along the length of the member. The results are given in Figs. 4.4 and 4.5 where the vertical axes are the elastic axial buckling load P_e divided by the axial load causing the yield of the full section P_y, and the elastic flexural buckling moment M_e divided by the moment causing initial yield at the extreme compression fiber of the full section M_y. Results show that instead of using full cross section properties to predict the overall buckling strength of perforated sections as assumed in the current design specification, better results can be obtained by using the weighted section properties for the torsional-flexural buckling and lateral buckling equation and the net section moment of inertia properties for the flexural buckling equation.

4.2   Member Strength

In order to deal with the presence of perforations in the column section, the RMI specification recommends the use of a stub column test to establish an effective net section. The area of the effective section is for an axially loaded member failing due to local behavior. The results are also further used to develop a reduction factor to find the effective section properties for bending and overall buckling. The objective of this study is to validate these reduction factors.

As in the previous study, the finite element method is used to predict the member strength. The analysis considers both geometric and material nonlinearities. Initial conditions of the model involve both flexural residual stresses and geometric imperfections. The magnitude of the flexural residual stresses throughout the thickness in the longitudinal direction is given in Fig. 4.2. These stresses are assumed to be tension on the outside and compression on the inside of the section. Geometric imperfection is introduced by using the buckling mode shape obtained from the buckling analysis. For short members where local or distortional buckling is critical, buckling mode shape with a maximum imperfection magnitude of one tenth of the thickness is used as the geometric imperfection. For long members where overall buckling is critical as shown in Fig. 4.2, the geometric imperfection is generated by superimposing the overall buckling and the local buckling mode shape together, where the maximum imperfection magnitudes of these modes are one thousandth of the member length and one tenth of the thickness, respectively. An idealization of the material model that is elastic-plastic with strain hardening is assumed where, $F_y = 45$ ksi, $F_u = 59$ ksi, $E = 29500$ ksi, $E_{st} = E/45$, $\nu = 0.3$ and e_{st} is 15 times the maximum elastic strain.

Results are compared with design specifications in Figs. 4.6 and 4.7. For the full sections, the initiation of the yielding procedure of the AISI specification is used while for the perforated sections the RMI specification is used. The RMI specification requires the use of the ultimate compression load from a stub column test. The finite element results for the concentrically loaded compression members are used in this case. For research purposes LRFD

is used here but with the resistance factors considered to be equal to one. It can be seen that both specifications give conservative results compared to the finite element method, especially for the very long length flexural members. According to the finite element solution, these members have postbuckling strength.

4.3   Development of a Design Approach for Beam-Columns

An interaction equation is used in the AISI specifications to design beam-columns. A finite element parametric study is carried out here to evaluate this equation. Column type A-LDR is used again with the same finite element assumptions as in the previous study but with modification of the applied load so that the members are subject to combined compressive axial load and bending about the strong axis. Three load cases with stress distributions applied at the ends of the member as shown in Fig. 4.8 are considered. The correlations of the finite element results with the interaction equation are given in Figs. 4.8 and 4.9. For a given finite element result, the members strength P_u and M_{ux} are substituted in the interaction equation and the resulting axial and flexural strength ratio is plotted. All the finite element results fall outside the triangle indicating that the interaction equation is conservative.

The interaction equation defines member failure by limitation on the combined strength ratio. The allowable member strengths $\phi_c P_n$, $\phi_b M_{nx}$ and $\phi_b M_{ny}$ are determined independently. Therefore, three separate failure modes must be considered, resulting in taking the lower bound limits of each governing strength. As seen from the finite element result, designing members with such an assumption can lead to rather conservative results, especially when failure by overall member instability takes place. An alternative design approach for beam-columns is presented here to improve the design efficiency. This proposed method represents the behavior of beam-columns by considering a single failure mode to govern the member capacity. The following are the design procedures. First, the combined axial and bending elastic critical buckling stress F_e for the member under the required load and boundary conditions is calculated.

$$F_e = \frac{P_e}{A} + \frac{M_{ex}}{S_x} + \frac{M_{ey}}{S_y}$$ (4.1)

where P_e is the elastic critical axial force, determined for an eccentrically loaded section, A is the cross-sectional area, S_x and S_y are the elastic section moduli for the extreme compression fiber about the x- and y-axes, M_{ex} and M_{ey} are the corresponding elastic critical moments about x- and y-axes. For beam-columns with equal end eccentricities, these moments are the end moments due to the eccentricity, e_y and e_x, respectively

$$M_{ex} = P_e e_y$$ (4.2)

$$M_{ey} = P_e e_x$$ (4.3)

The critical buckling load for an equal end eccentrically loaded section can be solved by using the computer program CU-TWP or by using the theoretical overall buckling equation given in Sarawit (2002). All the above parameters should be calculated based on the weighted section properties when designing perforated sections. The combined axial and bending nominal failure

stress F_n is then determined by interpolating between the two currently used design equations given in the AISI specification

$$F_n = \frac{\left(F_n\right)_P F_p + \left(F_n\right)_M \left(F_{mx} + F_{my}\right)}{F_p + F_{mx} + F_{my}} \tag{4.4}$$

where $\left(F_n\right)_P$ is the nominal failure stress for concentrically loaded compression members calculated according to the AISI Eqs. (C4-2) and (C4-3), with F_e determined from Eq. (4.1). $\left(F_n\right)_M$ is the nominal failure stress for flexural members calculated according to the AISI Eqs. (C3.1.2-2), (C3.1.2-3), and (C3.1.2-4), with the following notations substitution: $M_c = \left(F_n\right)_M$, $M_e = F_e$, and $M_y = F_y$. The axial buckling stress F_p and the bending buckling stresses F_{mx} and F_{my}, are fractions of the combined axial and bending buckling stress along the net cross section, computed as follows: $F_p = P_e/A_{net}$, $F_{mx} = M_{ex}/S_{xnet}$, and $F_{my} = M_{ey}/S_{ynet}$, in which A_{net} is the net cross-sectional area, S_{xnet} and S_{ynet} are the elastic section modulus of the net section for the extreme compression fiber about the x- and y-axes.

The reason for using Eq. (4.4) for beam-column designs is that the nominal failure stress determined from this expression is a weighted approximate value of the two current design equations as shown in Fig 4.3. The design equation for concentrically loaded compression member is the lower bound due to the consideration of the initial geometric imperfections and the design equation for flexural members is the upper bound due to the allowable additional beam capacity from the shape factor. The nominal failure stress determined from Eq. (4.4) should be reasonable because both the effects of the initial geometric imperfections and the additional capacity from the shape factor should be considered less in beam-columns.

The reduction factor for the net section, τ to account for local buckling, must then be calculated. By interpolating between the reduction factor expressions for concentrically loaded members and flexural members given in the RMI specification, the following expression is obtained for beam-columns:

$$\tau = 1 - \frac{(1-Q)}{2}\left(1 + \frac{F_p}{F_c}\right)\left(\frac{F_n}{F_y}\right)^Q \tag{4.5}$$

where

$$F_c = F_p + \frac{C_{mx}F_{mx}}{\alpha_x} + \frac{C_{my}F_{my}}{\alpha_y}$$

Q is determined by stub column tests according to the RMI specification. Definitions of C_{mx}/α_x and C_{my}/α_y are as given in the AISI specification. The nominal axial strength P_n is then determined as follows:

$$P_n = \tau A_{net}F_{np} \tag{4.6}$$

where $F_{np} = F_n F_p/F_c$ is the axial nominal failure stress. The corresponding nominal flexural strength M_{nx} and M_{ny} is then determined as follows:

$$M_{nx} = P_n M_{ex}/P_e \tag{4.7}$$

$$M_{ny} = P_n M_{ey}/P_e \tag{4.8}$$

Finally, with the AISI resistance factors, the design strengths are determined as follows:

$$P_u = \phi_c P_n \tag{4.9}$$

$$M_{ux} = \phi_b M_{nx} \tag{4.10}$$

$$M_{uy} = \phi_b \mathrm{M}_{ny} \tag{4.11}$$

Similar to the interaction equation this method also involves using the same moment magnification factor; therefore, some iteration is required to find P_u. That is, the assumed P_u used in α_x and α_y to solve Eq. (4.5) must be the same as when it is determined from Eq. (4.9). The net cross section properties are used in this approach to account for the perforations in the column sections. However, most perforated sections have more than one possible net section; therefore, the different net sections should be explored to find the least design strength. This proposed method for beam-column design is evaluated by comparing it with the previous finite element results and interaction equation as shown in Figs. 4.8 and 4.9. It can be seen that overall the proposed method works well for the torsional-flexural and flexural buckling agreeing better with the finite element results than the interaction equation.

4.4   Moment Magnification Factor

In the design of beam-columns, primary moments due to lateral loads and end moments are multiplied by moment magnification factors to account for the second order effects and the moment gradient in the member. This factor used in the current AISI specification is developed based on the assumption that failure by instability will be in the plane of bending. Thus, the current moment magnification factor does not consider the torsional-flexural failure mode. Generally this may not be the case. The torsional-flexural failure mode is common in thin-walled sections. If it takes place, the moments in the elastic beam-column will be unconservative if computed with the current moment magnification factor.

Peköz and Celebi (1969) presented an approximate analysis approach for elastic beam-columns with equal end eccentricities. Maximum bending moment in the member can be computed by using the member deformation results from this approach. When the column type A-LDR is subjected to a compression load with eccentricity $e_y = 1$ in. as shown in Fig. 4.10, the maximum bending moment about the strong axis $M_{x\max}$ computed from the Peköz and Celebi (1969) approach will not be the same as that from using the AISI moment magnification factor. As seen in Fig. 4.11 the AISI approach is unconservative. This is because the Peköz and Celebi (1969) approach has the level of P limited at the elastic critical axial load P_e, agreeing with the actual behavior in which the member will buckle by torsional-flexural at this load. But the AISI approach has it limited at the flexural buckling load P_{ex} instead. Contour plots given in Fig. 4.10 can be used to obtain P_e for the different load eccentricities.

5   COLD-FORMED STEEL FRAMES

The behavior of industrial storage racks depend on how the three individual components previously discussed: column bases, beam to column connections, and members perform interactively with each other. Thus the frame behavior can become very complex, many

parameters such as semi rigid nature of joints, presence of significant perforations, and susceptibility to local buckling are part of the cause. As to which analysis method is best to solve this problem will certainly depend on the tools available to the designer. The analysis model can be as simple as using a sub-structure model such as isolating the column and using the alignment chart, or as sophisticated as using numerical methods to analyze the entire frame. With the availability of powerful computers and software, the latter approach has become more attractive, allowing more complex and efficient designs to become possible. Current guidelines for analysis methods and design criteria are being reviewed in this research project. A preliminary study of finite element simulations of physical rack tests is illustrated here.

Physical tests of the pallet rack shown in Fig. 5.1 were conduced by Peköz (1975) for two loading cases. First, gravity loads were applied on each bay equally, and second, a combination of vertical and horizontal loads were applied. Horizontal loads at 1.5% of the vertical loads at each beam level were applied to the right at each beam to the column joint of the left upright frame. For the case of gravity loads, in the physical test, failure took place in the beams by yielding and local buckling. Complications arise when beam elements are used to model the shelf beams in this case. As shown in Fig. 5.2a, the finite element solution will yield unconservative results because beam elements did not accurately capture the local behavior.

For the case of the combination of vertical and horizontal loads, in the physical test, failure was due to sidesway collapse where most of the lag bolts were broken off due to the excessive rotation of the column bases. How the column bases are modeled are of great importance in this case. If simple linear torsional springs were used to model the column bases, even though the spring stiffnesses accurately represent the base fixity, satisfactory results are yet not possible as shown in Fig. 5.2b Model II. A double axial spring model as shown in Model I should instead be used in this case. A double axial spring model not only produces the same stiffness as the linear torsional spring but will also capture the upper bound limit of base fixities behavior. The physical result is higher than Model I indicating that the actual upper bound limit of the base fixity is slightly higher than assumed. Additional resistance from the base fixity could be due to the presence of the lag bolts. Currently different design approaches are being studied

6   SUMMARY AND CONCLUSIONS

This paper presents the results of four studies. The first study focuses on the column bases. Results show that the current base fixity equation underestimates the stiffness. Unless actual tests are conducted to obtain the base fixity, the proposed equation developed in this study along with the upper bound limits of the base fixity behavior should be considered. In the second study, a new beam to column connection test is presented. The proposed test may give a better understanding of the connections behavior and overcome the disadvantages of the current cantilever tests.

A critical review of the AISI and RMI design provision for cold-formed steel members was carried out in the third study. It was found that the overall elastic buckling strength of the perforated members could be predicted by using the weighted section properties for determining torsional-flexural buckling strength and lateral buckling strength and the net section moment of inertia properties for determining flexural buckling strength. Then sources of conservatism in the specification for the design of beam-columns were identified and a new design approach is presented to improve the results. The moment magnification factor was also looked at in this study. Determining the maximum bending moments by using the AISI moment magnification

factor is found to give unconservative results if the member failure is by torsional-flexural. Current research is focused on cold-formed steel frames. In this study current guidelines for analysis method and design criteria are being reviewed, and different possible analytical models are being studied.

ACKNOWLEDGEMENTS

REFERENCES

AISI, (1996). AISI Specification for the Design of Cold-Formed Steel Structural Members. American Iron and Steel Institute Washington, D.C.
Peköz, T., (1975). Pallet Rack Tests, Report submitted to Rack Manufactures Institute, Cornell University, Ithaca, NY.
Peköz, T., and N. Celebi (1969). "Torsional-Flexural Buckling of Thin-Walled Sections under Eccentric Load," Engineering Research Bulletin 69-1, Cornell University, 1969
RMI, (1997). Specification for the Design, Testing and Utilization of Industrial Steel Storage Racks 1997. Rack Manufactures Institute.
Salmon, C.G., Schenker, L. and Johnston, B.G., (1955). "Moment Rotation Characteristics of Column Anchorages", Proceedings, ASCE, April 1955.
Sarawit, A., (2002). Cold-Formed Steel Frame and Beam-Column Design, Progress Report submitted to the American Iron and Steel Institute and the Rack Manufactures Institute, Cornell University, Ithaca, NY.
Sokolnikoff, I.S., (1983). Mathematical Theory of Elasticity, Krieger Publishing Company, Malabar, Florida.

Table 2.1 Column and Base Plate Dimensions

bd, in.^{2}	d/b	c, in.	t_w, in.	t_p/t_w
4, 6.25, 9, 12.25, 16, 20.25, 25, 30.25, 36	1, 1.25, 1.5, 1.75, 2	0, $d/2$	0.05, 0.10	1, 1.5, 2, 2.5, 3
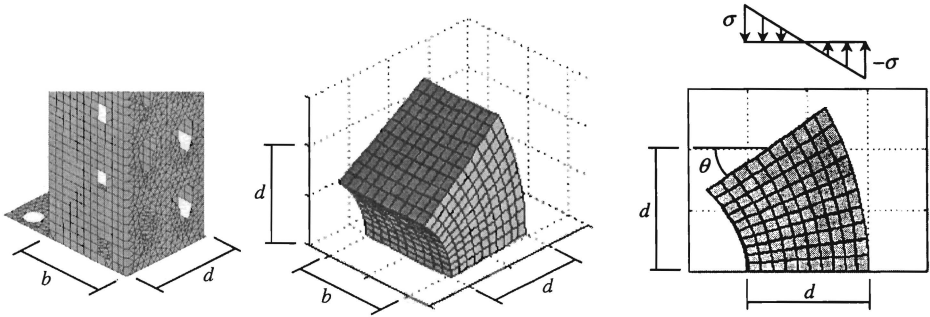
Fig. 2.1 Deformation shape of the concrete block under the base plate
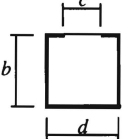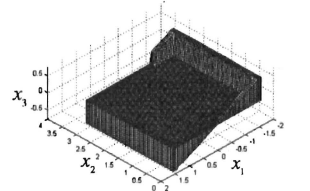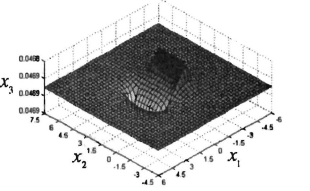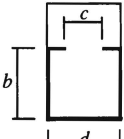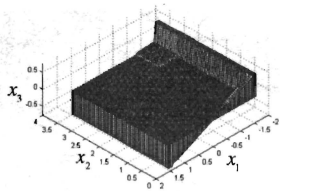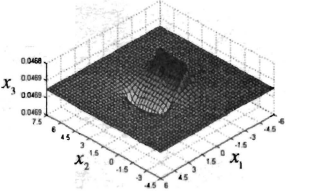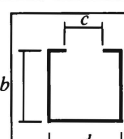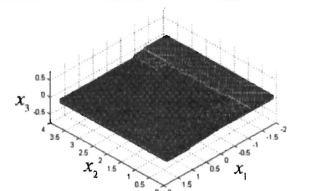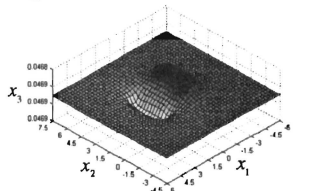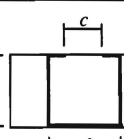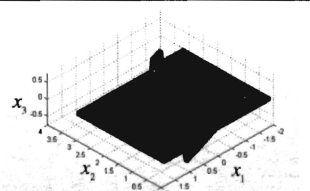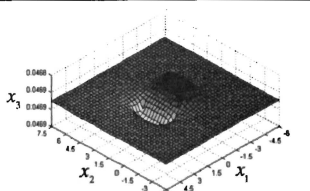
Base Plate	Normal Loads Distribution	Concrete Surface Deformation
Type A		
Type B		
Type C		
Type D		

Fig. 2.2 Base plate configurations
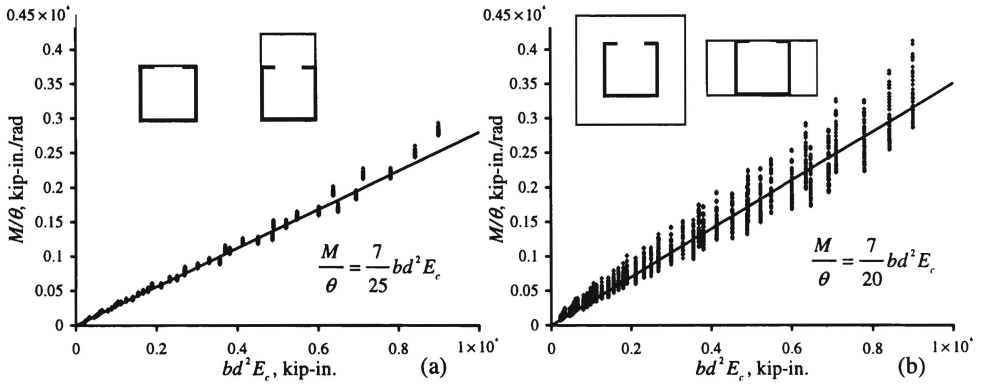
Fig. 2.3 Base fixity (a) Base plate type A & B (b) Base plate type C & D

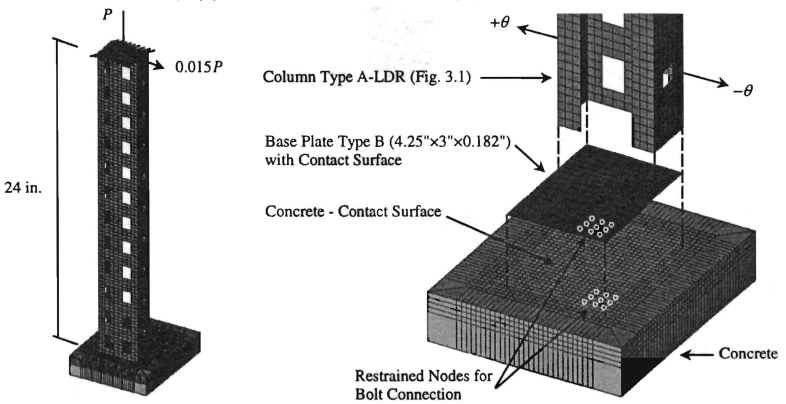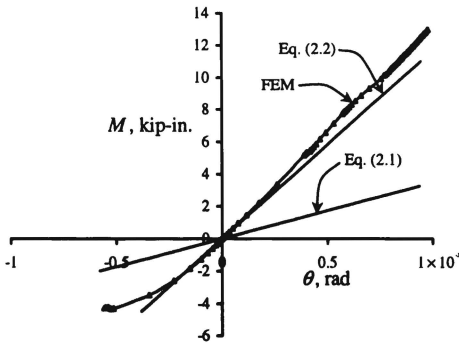For figure (a):

$$\frac{M}{\theta} = \frac{7}{25}bd^2E_c$$

For figure (b):

$$\frac{M}{\theta} = \frac{7}{20}bd^2E_c$$

Fig. 2.4 Column Base Finite Element Model

Fig. 2.5 Comparison of base fixity Eqs. with FEM results   Fig. 3.1 Cantilever test
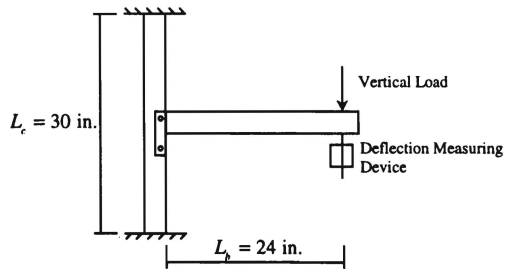
Fig. 3.2 Portal test

Thick-walled section: $t = 0.091$ in.
Thin-walled section: $t = 0.045$ in.

Full Section

Net Section I

Net Section II
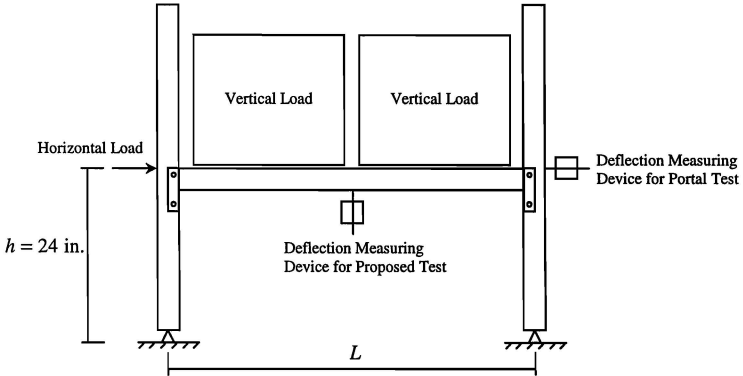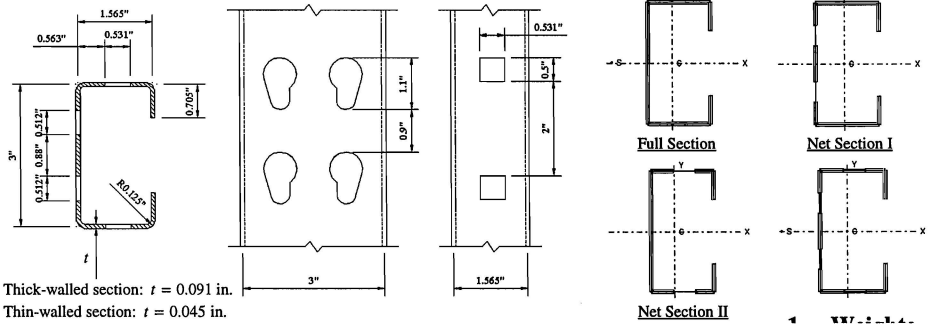
Fig. 4.1 Column Type A-LDR Dimensions

Bending residue stresses

Geometric imperfections: Local buckling   Overall buckling
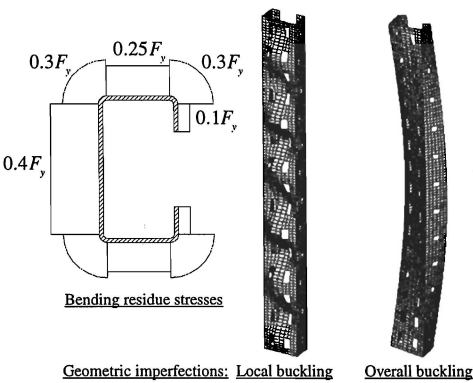
Fig. 4.2 Initial conditions for the model
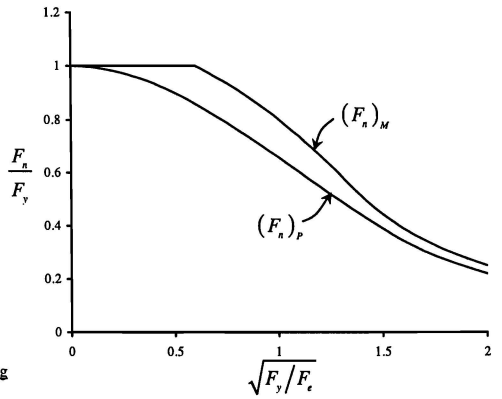
Fig. 4.3 Comparison of design equations
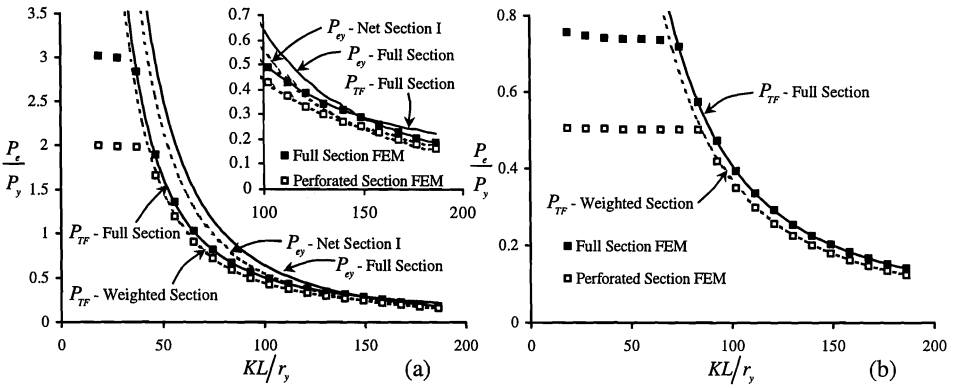
Fig. 4.4 Elastic buckling axial load (a) Thick-walled section (b) Thin-walled section
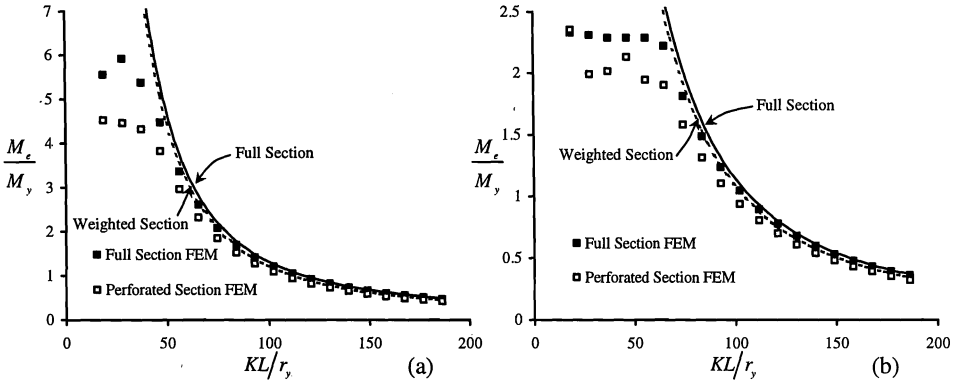
Fig. 4.5 Elastic buckling moment (a) Thick-walled section (b) Thin-walled section
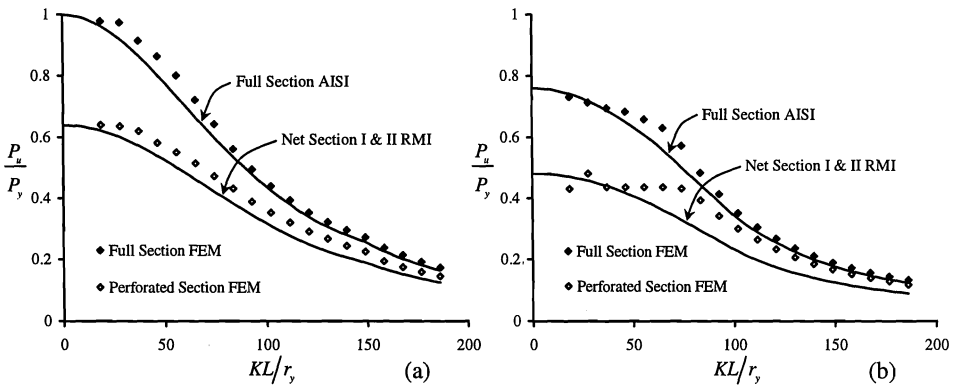
Fig. 4.6 Compressive axial strength (a) Thick-walled section (b) Thin-walled section

Fig. 4.7 Flexural strength (a) Thick-walled section (b) Thin-walled section

Fig. 4.8 Full section beam-column strength (a) Thick-walled section (b) Thin-walled section

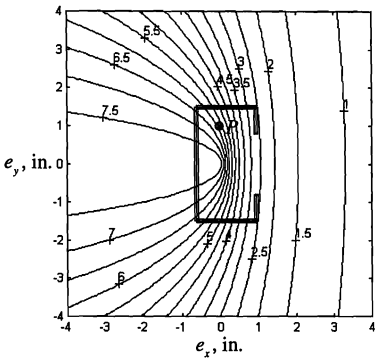Fig. 4.9 Perforated beam-column strength (a) Thick-walled section (b) Thin-walled section
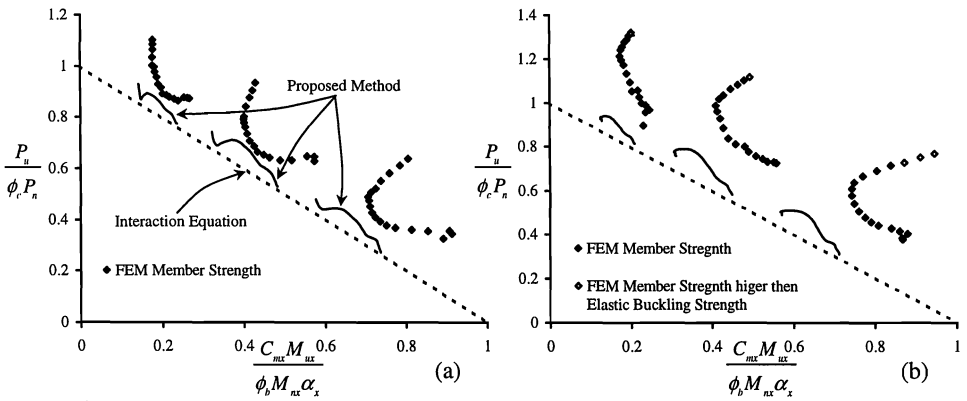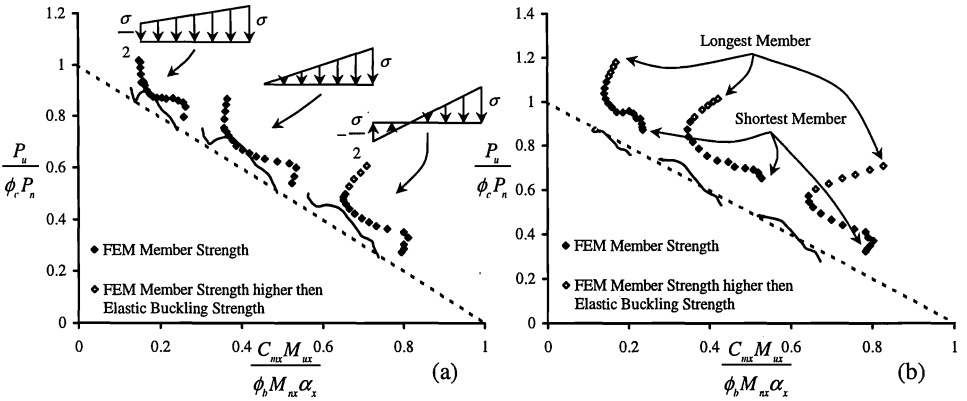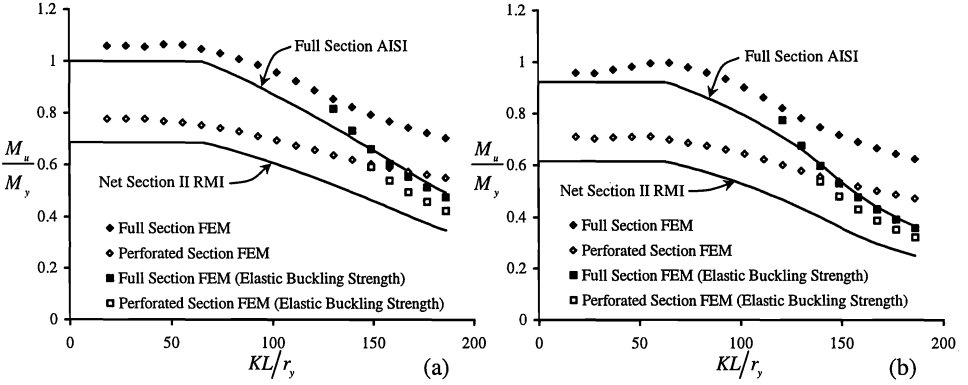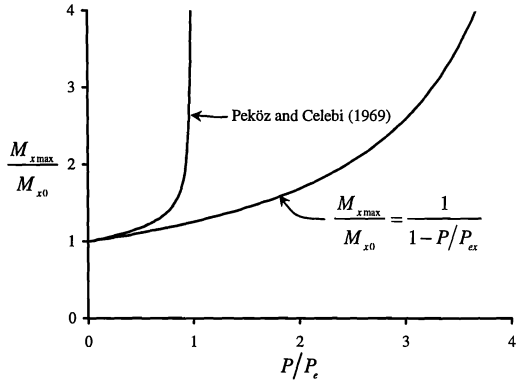
Fig. 4.10 Elastic critical axial force P_e, kips   Fig. 4.11 Comparisons of moment magnifications
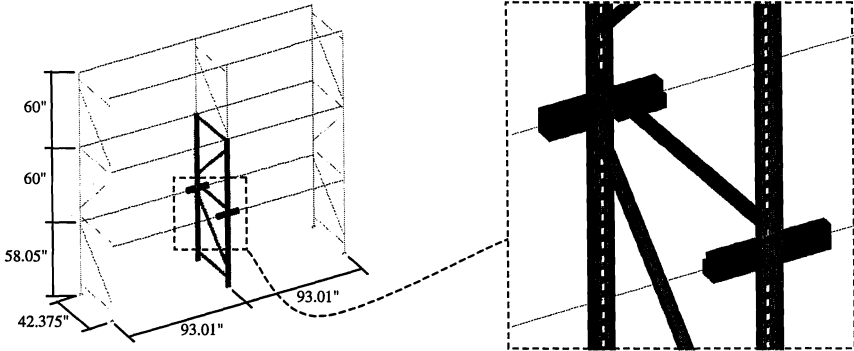

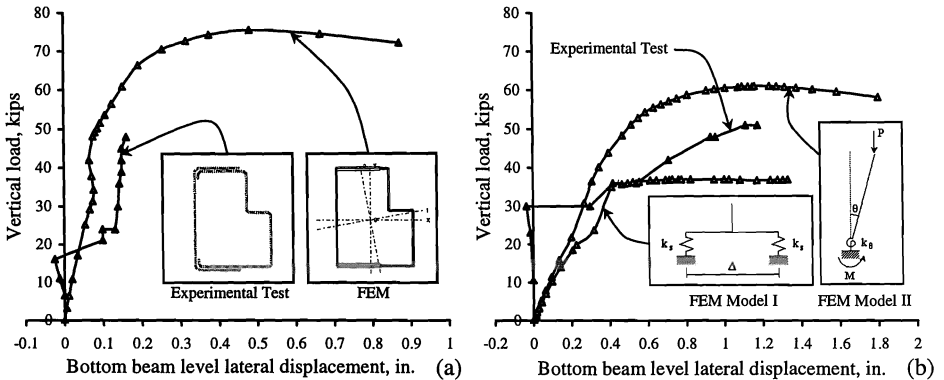Fig. 5.1 Storage rack type A-LDR Finite element model

Fig. 5.2 Comparison of test and FEM results (a) Gravity loads (b) Vertical + Horizontal loads